Plastic deformation and post-deformation annealing in chromite: mechanisms and implications

(Revision 5)

Biswajit Ghosh[1,3]*, Santanu Misra[2], Tomoaki Morishita[3]

[1]*Department of Geology, University of Calcutta, 35 Ballygunge Circular Road, Kolkata, India*
[2]*Department of Earth Sciences, Indian Institute of Technology, Kanpur, UP-208016, India*
[3]*School of Natural System, College of Science and Engineering, Kanazawa University, Japan*

Abstract

Plastic deformation in chromite is not frequently reported in literature. We present a detailed microstructural analysis of this mineral from massive chromitite of the Neoarchaean Sittampundi Complex, southern India. The study reveals intracrystalline plasticity is dominantly active in this mineral and it produces distinctive features corresponding to at least two different microstructural regimes. The Regime 1 is deformation-related and it commenced with recovery of strained grains and formation of new grains, corresponding to subgrain rotation recrystallization. This was followed by nucleation of strain-free new grains in regions of high strain. The Regime 2 appears to be post-deformational and dominantly temperature-controlled, producing distinctive features of static annealing of already deformed grains. This regime corresponds to grain boundary migration recrystallization resulting coarsening of strain-free facetted, new grains at the expense of high dislocation density subgrains. The resultant micro-features resemble closely what is known as '*abnormal grain growth*', not yet documented for chromites. These coarse grains, in places, also feature accommodation of deformation by displaying very low angle subgrain boundaries. The movement of high-angle grain boundaries in Regime 2 through precursor strained grains provided high diffusivity paths for the rapid exchange of components, producing compositional heterogeneity between grains dominated by deformation features and facetted, new grains. These microstructural observations coupled with chemical heterogeneity provide new directions in interpreting the deformation mechanism of chromite, and its annealing history at the post-deformation stage.

Keywords: Chromite, Plastic deformation and recrystallization, Strain-free new grain, Annealing, Abnormal grain growth.

**Corresponding Author. E-mail: bghosh_geol@hotmail.com Tel: +91-33-2461-4891*

INTRODUCTION

The general absence of substructures in chromites from mantle peridotites and chromitites (Christiansen, 1985) and subsequent recognition of stress-induced Al-Cr multipolar zoning in ophiolitic chromites prompted to believe that dislocation creep is not a dominant mechanism in the deformation of chromite (Ozawa, 1989). Instead, diffusion creep is thought to be the principal mechanism in its deformation. The lack of appreciation of chromite crystal plasticity owes to the fact that chromite, among the cubic minerals, has low stacking fault energy, like garnet, and hence struggles to develop dislocation based microstructures. While using backscatter electron (BSE) channeling pattern and orientation contrast in scanning electron microscopy, chromites from Oman ophiolite have served to provide evidences favoring limited dislocation creep mechanisms at high temperature during mantle flow (Christiansen, 1986), well constrained natural examples of crystal-plastic deformation in the dislocation creep regime were absent until recently, when Vukmanovic et al. (2013) described chromite microstructures in the stratiform chromitite layer from the Meerensky Reef. Soon after, chromite crystal plasticity was documented from podiform mantle chromitites in ophiolitic setting (Ghosh et al., 2014). Very recently fluid-assisted chromite deformation, promoting chemical and textural modification has also been reported (Satsukawa et al., 2015a).

Our study focuses on trench samples of foliated stratiform chromitites (Fig. 1a) occurring as seams containing 60–70 modal% of porphyroclastic chromites with the remaining matrix, constituted dominantly by amphiboles, mainly tschermakitic hornblende with accessory phlogopites from the Sittampundi Layered Complex (SLC), southern India which is thought to be equivalent to Fiskenaesset complex of West Greenland (Ghisler, 1970). The SLC is a deformed, anorthosite-dominated layered igneous complex within Palghat–Cauvery Shear Zone

(PCSZ) that represents a geosuture amalgamating two crustal blocks (Santosh et al., 2009; Santosh and Kusky, 2010) with different isotopic characteristics, age, structure, metamorphism and magmatism (Meissner et al., 2002). The SLC was formed in Neoarchaean (Bhaskar Rao et al., 1996) and was subjected to eclogite facies metamorphism (>1000 °C and >20 kbar) corresponding to 65 km paleo-depth, near to the crust-mantle boundary and later exhumed in the latest Neoproterozoic–Cambrian (Sajeev et al., 2009). Structurally, the Sittampundi complex was initially considered as a single stratigraphic unit (Subramanian, 1956; Naidu, 1963). A detailed work (Ramadurai, 1975) later, however, suggested that the complex consists of a repeated stratigraphic sequence resulted from a tight (isoclinal) anticline structure of the region.

In order to know the impact of deformation at such high pressure and temperature on chromites, we carried out a detailed microstructural study on chromitites sampled from different stratigraphic horizons using high resolution optical microscopy, Back Scattered Electron (BSE) imaging, quantitative chemical analysis, elemental mapping and Electron Back Scattered Diffraction (EBSD) techniques. Our results imply that chromite, like pyrite, is more ductile than generally inferred (Barrie et al., 2010), and we demonstrate the intracrystalline plastic deformation mechanisms in this mineral. We have identified two distinct microstructural regimes; Regime 1 and Regime 2 based on characteristic features and attributed them as functions of relative magnitude of deformation and temperature respectively. This work differs from related one, performed experimentally on other minerals in that our observations here is made on natural samples and not constrained in controlled conditions exclusive to each of these microstructural regimes and to their transitions. Therefore, the observations made here are based entirely on relict micro-features arrested in some grains.

SAMPLING AND ANALYTICAL METHODS

Based on estimation of intensity of foliation observed in the field and their outcrop location, we collected 12 samples, 4 from each 3 different chromitite seams (KPT5: N11°16'04", E77°59'58", BL-SII: N11°14'17", E77°57'21" and CPT6: N11°15'40" E77°58'56") corresponding to different stratigraphic horizons around Karungalpatti area (Fig. 1b). We initially analyzed all of them on thin sections cut perpendicular to foliation (Fig. 2a) for BSE imaging, and based on the output we finally selected 3 samples, each representing a seam for detailed quantitative orientation analysis (EBSD) analysis. We emphasis here that the observed micro-features (see next) corresponding to two regimes (Regime 1 and 2, discussed later), do not occur in all the seams. Those related to the Regime 1 are restricted to seams at the upper and middle horizons (sample locations KPT5 and BL-SII, respectively) whereas, those related to the Regime 2 are specific only to the bottom horizon (sample location CPT6). However, some features of Regime 1 are preserved in samples that exhibit regime 2 features.

BSE imaging, quantitative chemical point analysis and elemental mapping were carried out at Kanazawa University, Japan using an electron probe micro-analyzer (JEOL JXA-8800 Superprobe). The analyses were performed under an accelerating voltage of 15 kV and beam current of 20 nA, using a beam diameter of 3 μm. EBSD analysis was carried out at Electron Microscopy Center at ETH, Zurich (EMEZ) with FEI Quanta 200. The chromitite samples were cut perpendicular to the foliation (A2-A3 plane, Fig. 2a), impregnated in epoxy and polished for EBSD analysis. The EBSD patterns and data were generated by the vertical incidence of electron beams on the polished surface of the sample, tilted at 70° with respect to the horizontal plane of the scanning electron microscope. The scheme of the sample orientation with respect to the EBSD analysis is shown in Figure 2. The acceleration voltage and probe current were set at 20

kV and 8.2 (±0.2) nA, respectively and the working distance was 18-20 mm. Diffraction patterns were automatically collected with 40-45 fps, indexed (initial indexing rate ~ 90%) and analyzed using an orientation imaging microscopy software (TSL OIM) from the quadrangle areas of the samples, using step sizes of 5 or 7 μm (depending on the average grain size of the region being mapped). The automatic data processing converted non-indexed data-points (pixels) to indexed with respect to the index-patterns of the neighbouring pixels. Only data with a high level of reliability (confidence index CI >0.2) were used in the statistical orientation analysis presented in this paper. A series of TSL OIM built-in "clean-up" steps were used to replace non-indexed data points with reliable orientations from the neighbouring pixels. For grain dilation default 5° grain tolerance angle and 2 pixels minimum grain size were set under single iteration. A similar protocol applied for Grain CI and grain fit standardizations. For neighbour CI and orientation correlations the minimum confidence index was set to 0.2.

In the following discussions related to EBSD analysis we have presented three major map types – i) Image Quality (IQ), ii) Inverse Pole Figure (IPF) and iii) Kernel Average Misorientation (KAM) maps. The IQ maps show the quality of the diffraction pattern obtained during a scan, and thus they provide information and visualization of microstructures, particularly the misorientation of the grains. In our analysis we have defined boundary as any adjacent point pair with misorientation exceeding 2°. We have mapped the boundaries in three segments – subgrains (misorientation-boundaries ≤ 5°); intermediate grains (misorientation-boundaries from 5-15°) and recrystallized grains (misorientation-boundaries ≥ 15°). The recrystallized grains may have partial subgrain/intermediate grain boundaries. They are apparently strain-free with internal misorientations less than 1-2°. The IQ maps are highlighted to show several analytical directions (transects) used in this study. The IPF maps are color-coded

based on the orientation of the grains. Red, green and blue colors are designated to grains whose <100>, <110> and <111> axes, respectively, are parallel to the projection of the IPF. All other orientations are color-coded and are assigned blends of these three basic colors based on orientation. The IPF maps are projected along the z direction, which is equivalent to A1 (Fig. 2a) of the sample geometry. Like the IQ maps the IPF maps are also highlighted with the grain boundaries. The KAM maps obtained from the EBSD data reveal the average misorientation angle at any point taking into account of all the neighbouring analysis points. We have selected up to 10th nearest neighbours with maximum misorientation angle of 5°. The KAM maps are useful to interpret the internal strain which is represented by concentration of low angle boundaries. We have also made profiles across grains to show change in orientation relative to the starting point along specific directions.

OBSERVATIONS

Based on the pattern and the mutual disposition of grains we have classified the observed microstructures in two major regimes. The Regime 1 shows significant change in orientation within individual grains with presence of subgrain boundaries. The Regime 2 is characterized by abundance of large (~ 300-400μ) grains that exhibit little to no crystal lattice bending and straight grain boundaries. A detailed account of the observed microstructures is provided below.

Regime 1

The porphyroclastic chromite grains of the upper chromitite seam (KPT5) are little deformed and do not show much evidence of intra-grain lattice distortion (recovery) except at the marginal part (Figs. 3 and 4). These grains seldom preserve micro-fractures within them. The IQ, IPF and KAM maps illustrate low angle grain boundaries within the parent grains (Figs. 3A-C

and 4A-C). The texture-component maps (Figs. 3D and 4D) were prepared by considering orientations ranging within 30° from the orientation of the parent grain measured at the center. These maps reveal that the edges of the parent grains are represented by subgrains. The recrystallized grains are little larger than the subgrains. They are characterized by 120° triple junction boundaries and display both daughter and neighbor-daughter dispositions (Halfpenny et al., 2006; Fig. 4) with comparable size range. The misorientation angle data measured from the central part of the parent grains to their edge reveal a maximum deviation of about 10° (Figs. 3E and 4E). The profiles show distinct plateaus in some subgrains but also continuous lattice bending.

The chromitite samples collected from the middle horizon (BL-SII) are more deformed compared to the KPT5 samples; also correspond to Regime 1. The shape of the precursor porphyroclastic grains is slightly elongated and the aggregate of smaller grains appears like ribbon. The outer margin of individual precursor grain shows highest concentration of substructures of similar size range, which gradually diminishes towards the inner part (Figs. 5 and 6). The parent grains are internally strained with development of low angle misorientations within them (Figs. 5A, B and 6A, B). They show an overall increase in misorientation from their centres to the rims (Figs. 5D, E and 6D, E). The recrystallized grains are relatively larger, compared to those observed in KPT5 and have internal misorientations less than 1° (Fig. 5E, inset). Here too the boundaries between the substructures are commonly straight and form 120° triple junctions (Fig. 5C, arrowheads). The recrystallized grains are bounded partly by high-angle and partly by subgrain/intermediate grain boundaries. All these substructures commonly surround the relict of the precursor grain (parent), giving rise to typical core-mantle structure. Following the nomenclature by Halfpenny et al. (2006) the neighbor-daughters are mostly

subgrains and/or intermediate grains and the daughters are new recrystallized grains. Further, the daughters and the neighbor-daughters have comparable size range. Another set of new grains with very high-angle grain boundaries (>15°) begin to form next in the sequence in this regime near the rims of the parent grains i.e., the regions of high strain (Fig. 6A, arrowheads). The regions of high strain are marked by high crystal lattice bending as evident in KAM map (Fig. 6C). These grains are typical in the sense that they occur within the parent grains not similar to those of daughters and are inclusion-free. Part of the grain boundaries of these grains are straight (idioblastic) and other sections are serrated. Similar inclusion-free recrystallized grains of chromite were reported earlier from the Fiskenaesset deposit of West Greenland (Ghisler, 1976), Oman ophiolite complex (Christiansen, 1985) and recently from Luobusa ophiolite (Satsukawa et al., 2015b).

Regime 2

The chromitite seams at the bottom horizon (CPT6) are intensely deformed corresponding to Regime 2 (Figs. 7 and 8). The relict precursor grains are mostly occupied by subgrains whereas, the peripheral parts are decorated by dynamically recrystallized chromite grains of smaller grain size (Figs. 7A, B and 8A, B). The KAM maps (Figs. 7C and 8C) also support the observation that the parent grains are relatively more deformed compared to those of KPT5 and BL-SII samples. The misorientation data from core to the grain boundaries show a gradual increase, however with sudden jumps (Figs. 7F and 8D). The most interesting observation in these samples is abundance of relatively large strain-free faceted grains (Figs. 7 and 8). These large idioblastic and faceted (Fig. 7 D, E) grains are different from the grains with significant internal crystal bending (e.g. high KAM values) and are bounded by both straight and serrated grain boundaries. The misorientation data across these large grains reveal maximum

misorientation deviation less than 1° (Figs. 7E inset and 8E). However, there are occasional presence of feeble substructures within the large grains (Fig. 8F).

A compositional distinction at this regime between the large idioblastic crystals and the remains of the precursor grain is documented earlier (Ghosh and Konar, 2012). This distinction is evident from the tonal difference in the high contrast BSE image (Fig. 9). In terms of elemental distribution these new large grains contain less Cr and more Al in comparison to the parent grains which is also reflected in their Cr# [= Cr/(Cr + A1) atomic ratio] values whereas, the correlation with Mg and Fe is not so apparent (Fig. 9).

DISCUSSION

The microstructures in Sittampundi chromites revealed distinct domains with characteristic features. The changing microstructural pattern as evident from the characteristic features corresponding to two regimes might be attributed to deformation and temperature gradient as well. Given the scale of the field area and previous studies there is no strong evidence to justify that these two factors were mutually exclusive, however, there could be dominance of one over another in respective regions, the reason of which is still unknown. The deformation event might have followed by heating or some fluid influx at least in the local scale.

Origin of Regime 1

The Regime 1 is deformation related and the dominant strain accommodating mechanism commenced with recovery-accommodated dislocation creep (Tullis and Yund, 1985). Because of increasing ease of diffusion in the crystal lattice in this regime and owing to faster mobility of newly formed dislocations, the plastic deformation commenced with the onset of recovery that eventually lead to subgrain rotation recrystallization in presence of deformation (Figs. 3 - 6). The

primary evidence for subgrain rotation recrystallization is core and mantle structure, where the cores of precursor grains pass out transitionally into the mantle with increasing subgrain development and misorientation (Halfpenny et al., 2006; 2012), which is the case for Sittampundi chromites in Regime 1. Additionally, the increasing misorientation angles from the core to the boundary of the parent grains justify the mechanism of subgrain roration recrystallization in this domain. The presence of distinct plateaus with continuous lattice bending in the profiles speaks strongly in favour of ongoing progressive recrystallization and crystal plasticity. This recrystallization process is an extension of the recovery where the driving force is a reduction of the internal strain energy of the deforming aggregate. Dislocation climb perhaps dominated over glide alike garnet deformation in this regime (Prior et al., 2000). In terms of kinetics, Regime 1 was purely rotational and temporally continual, persistent until the end of deformation (Drury and Urai, 1990).

Origin of Regime 2

From the general lack of substructures in large strain-free grains the Regime 2 appears to be post-deformational and is dominantly temperature controlled. These relatively large crystals are often bounded by straight grain boundaries indicating lower internal free energy prevailing along those straight growth-lines and thus can be termed qualitatively as faceted grain boundaries (Gottstein and Shvindlerman, 2010). A quantitative analysis of two such grains (Fig. 7 D, E) also shows the face parallel grain growth. The microstructural features in this regime closely resemble what is known in the literature as ‘abnormal or exaggerated grain growth’ (Kang, 2005; Omori et al., 2013), also referred to as ‘discontinuous grain growth’ (Stockhert and Duyster, 1999), commonly related to annealing of pre-deformed grains. In this regime rotational and migration related recrystallization process operated simultaneously. Regime 2 is

discontinuous, in contrary to the earlier regime. This discontinuous nature of the migration related recrystallization produced large strain-free regions in the microstructure which was likely favored by solute escape from the high-angle migration front. The growth morphology of the boundaries of new grains was controlled by interfacial energy of cubic crystals as evident from their polygonal habit. However, the occasional presence of feeble substructures within the large faceted grains (Fig. 8) either signifies a continuum of their growth at the very end stage of deformation or it demonstrates growth related defects (Piazolo et al., 2005). As a whole the Regime 2 characterizes microstructural features of static annealing conditions of already deformed grains. During this stage the stored free energy of such system is reduced through vacancy diffusion and also grain growth which is facilitated by grain boundary migration (Baker, 2000). In general, grain boundary migration is driven by curvature which is related to the requirement to reduce total boundary surface area, and also strain energy which is related to the difference in unbound dislocation density either side of a boundary (Piazolo et al., 2006). Since, grain growth driven by reduction of grain boundary energy becomes the dominant process only when all grains are relatively dislocation-free (Humphreys and Hatherly, 1995; Urai et al., 1986), the driving force in Regime 2 for Sittampundi chromites originated partly due to a difference in the dislocation density across the grain boundary (Hirth and Tullis 1992). However, in solid solution minerals, grain boundary migration is not only driven by internal strain energy, but also by chemical driving potentials in terms of compositional changes of minerals associated with dynamic recrystallization (Kirby and Kronenberg, 1984; Urai et al., 1986; Berger and Stunitz, 1996; Passchier and Trouw, 2005). Since there is a compositional difference between crystals of the same phase on either side of a migrating boundary chemical free energy might have played a significant role in considering the driving force in this regime. This process is referred to as

diffusion-induced grain boundary migration (DIGM) (Hay and Evans, 1987). The kinetics of migration depends upon the magnitude of the driving force and the boundary mobility, which in turn is function of boundary structure, impurity effects and fluid effects (Urai, 1983).

Origin of strain-free grains

The formation of strain-free new grains might occur in deformed minerals by subgrain growth in regions of high dislocation density. Such development has been reported from natural rocksalt samples (Desbois, 2010) and also experimentally revealed in case of feldspar (White, 1975), pyrite (Cox et al., 1981), olivine (Toriumi and Karato, 1985) and also in synthetic rocksalt (Piazolo et al., 2006). Recrystallization in all these experiments involved a progressive stage of new high-angle grain boundary formation by subgrain rotation, followed by a stage of new grain development along newly-formed grain boundaries. However, because of the strain-free grains in our samples do not always occur in subgrain-rich domains and the general lack of evidences of dominant subgrain growth, classical nucleation recrystallization may be considered as a possible alternative where a cluster of atoms spontaneously takes on a new orientation owing to the action of thermally activated fluctuations. It is more likely because chemical driving forces were also involved (Hay and Evans, 1987; Etheridge and Hobbs, 1974).

Compositional heterogeneity

Deformation might increase the rate of compositional exchange between minerals (Yund and Tullis, 1991). Stress induced kinetic demixing of solid solution minerals is reported for feldspar (Yund and Tullis, 1991), amphibole (Stunitz, 1998), pyroxene (Stunitz, 1998), olivine (Hirth and Kohlstedt, 1995), garnet (Wang and Ji, 2000; Storey and Prior, 2005; Bestmann et al., 2008; Smit et al., 2011) and chromite (Ozawa, 1989; Sammis, 1989). We describe the change in

composition across the high-angle grain boundaries of the faceted strain-free new grains in our samples in terms of chemical diffusion which is a temperature sensitive process. These grains after their nucleation at the end of Regime 1 grew by outward grain boundary migration all through the next regime, which was likely to be a higher temperature event. Volume diffusion (Nabarro-Herring creep) is more effective for relatively finer grain size because of ease of travelling shorter distances. Considering the relatively larger sizes of the faceted strain-free grains in our samples we propose the model of grain boundary diffusion (Coble creep) to explain the elemental reequilibration (Fig. 10). During recrystallization the high-angle grain boundaries sweep through strained grains to remove dislocations and possibly subgrain boundaries (Passchier and Trouw, 2005; Hay and Evans, 1987). It is equally applicable even for temperature-induced grain boundary migration in static recrystallization. This movement of high-angle grain boundaries through strained grains provides high diffusivity paths for the rapid exchange of components, like Al - Cr during deformation and this might have produced compositional heterogeneity in the recrystallized grains. Interestingly, the relatively small recrystallized grains which were produced by progressive subgrain rotation during recovery-accommodated dislocation do not show compositional reequilibration because they were not swept by high-angle grain boundaries (Stunitz, 1998).

Thus, high mobility of preexisting dislocations during annealing in a later heating event might have promoted grain boundary migration and thereby facilitating diffusion, which in turn induced grain boundary migration. This perhaps defined a cause and effect loop in this process and once boundary migration initiated because of some other means, like contrast in dislocation density across the boundary, it became self-driven in the rest of the deformation.

IMPLICATIONS

Although of low average modal abundance, chromite is a significant mineral phase considering the chromium reservoir of the bulk earth, the upper mantle in particular. The identification and characterization of deformation mechanisms in this mineral are of interest because these mechanisms govern the rheological response of chromite dominated rocks (viz. chromitite) (Frost and Ashby, 1982). For example, deformation via dynamic recrystallization will result in strain softening (Poirier, 1985). The composition of chromite is widely used as i) a petrogenetic and geotectonic indicator (Dick and Bullen, 1984), ii) a geospeedometer (Ozawa, 1985), iii) a geothermometer (Fabries, 1979) and also iv) an oxygen geobarometer (Wood and Virgo, 1989). While subsolidus and/or metamorphic reequilibration is taken into account in many instances, the core compositions of large chromite grains from massive chromitite are considered unaffected because of the notion that massive chromitite minimizes the effects of reequilibration with adjacent silicates (Suita and Streider, 1996). Our study on Sittampundi massive chromitites demonstrates how deformation may induce intra-phase compositional reequilibration in chromite, producing compositional heterogeneity throughout. This constrains on extensive use of chromite composition in many petrologic studies without much adherence to microstructural consideration which in most of the cases are lacking. This lacuna is mainly due to the fact that chromite is isotropic and predominantly opaque, posing difficulties in recognizing the substructures during routine microscopic studies. We emphasize the importance of a reconnaissance microstructural study using orientation contrast imaging before applying its composition for petrologic purposes. Further, annealing microstructures from geological samples are not commonly reported. This study on Sittampundi chromites stands as a natural example of recognizing behavior of this mineral during deformation and also in post-deformational heating

event, not yet documented in the literature. Proper identification of annealed microstructures in massive chromitite is immensely important because extreme development of the faceted new grains in association with other recrystallized grains with 120° triple junctions may give rise to a pseudo adcumulate texture, common to many early magmatic rocks.

Summarizing, this study provides an account of plastic deformation mechanism of chromite from natural samples that substantially enhances our understanding of the physiochemical behavior of this mineral at the crust-mantle boundary. Whilst this study was unable to set the limits of natural variables at the transitions of successive microstructural regimes it leaves a scope for further experimental investigations to constrain these parameters well in preparing the deformation mechanism map for this mineral.

ACKNOWLEDGEMENTS

The authors thank Zoja Vukmanovic and one anonymous reviewer for their insightful comments and suggestions that improved the quality of the text and figures. Editorial handling and constructive criticism by Sandra Piazolo is greatly acknowledged. Shashank Shekhar is acknowledged for his critical reading of the manuscript. Karsten Kunze from Scientific Center for Optical and Electron Microscopy (ETZ Zurich) assisted in obtaining and analyzing the EBSD data. B.G. acknowledges the financial support received from UGC-DRS Phase-II, 2013-18, Government of India and JSPS Invitation Fellowship (FY 2015). SM thanks the infrastructural facilities provided by IIT Kanpur.

REFERENCES CITED

Baker, I., (2000) Recovery, recrystallization and grain growth in ordered alloys. Intermetallics, 8, 1183–1196.

Barrie, C.D., Boyle, A.P., Cook, N.J., and Prior, D.J., (2010) Deformation mechanisms and textural changes in pyrite (FeS_2) in the massive sulphide deposits of the Norwegian Caledonides. Tectonophysics, 283, 269–286.

Berger, A., and Stunitz, H., (1996) Deformation mechanisms and reactions of hornblende: examples from the Bergell tonalite (Central Alps). Tectonophysics, 257, 149-174.

Bestmann, M., Habler. G., Heidelbach. F., and Thöni, M., (2008) Dynamic recrystallization of garnet and related diffusion processes. Journal of Structural Geology, 30, 777–790.

Bhaskar Rao, Y.J., Chetty, T.R.K., Janardhan, A.S., and Gopalan, K., (1996) Sm–Nd and Rb–Sr ages and P –T history of the Archean Sittampundi and Bhavani layered meta-anorthosite complexes in Cauvery shear zone, South India: evidence for Neoproterozoic reworking of Archean crust. Contributions to Mineralogy and Petrology, 125, 237–250.

Christiansen, F.G., (1985) Deformation fabric and microstructures in ophiolitic chromitites and host ultramafics, Sultanate of Oman. Geologische Rundschau, 74, 61–76.

Christiansen, F.G., (1986) Deformation of chromite: S.E.M. investigations. Tectonophysics, 121, 175-196.

Cox, S.F., Etheridge, M.A., and Hobbs, B.E., (1981) The experimental ductile deformation of polycrystalline and single crystal pyrite. Economic Geology, 76, 2105-2117.

Desbois, G., Zavada, P., Schleder, Z., and Urai, J.L., (2010) Deformation and recrystallization mechanisms in actively extruding salt fountain: Microstructural evidence for a switch in

deformation mechanisms with increased availability of meteoric water and decreased grain size (Qum Kuh, central Iran). Journal of Structural Geology, 32, 580-594.

Dick, H.J.B., and Bullen, T., (1984) Chromian spinel as a petrogenetic indicator in abyssal and alpine-type peridotites and spatially associated lavas. Contributions to Mineralogy and Petrology, 86, 54–76.

Drury, M.R., and Urai, J.L., (1990) Deformation-related recrystallization processes. Tectonophysics, 172, 235-253.

Etheridge, M.A., and Hobbs, B.E., (1974) Chemical and deformational controls of recrystallization of mica. Contributions to Mineralogy and Petrology, 43, 111-124.

Fabries, J., (1979) Spinel-olivine geothermometry in peridotite from ultramafic complex. Contributions to Mineralogy and Petrology, 69, 329-336.

Frost, H.J., and Ashby, M.F., (1982) Deformation-mechanism Maps. The Plasticity and Creep of Metals and Ceramics. Pergamon Press, New York.

Ghisler, M., (1970) Pre-metamorphic folded chromite deposits of stratiform type in the early Precambrian of West Greenland. Mineralium Deposita, 5, 223–236.

Ghisler, M., (1976) The geology, mineralogy and geochemistry of the pre-orogenic Archaean stratiform chromite deposits at Fiskenaesset, West Greenland. Monograph Series. Mineralium Deposita, 14, 156.

Ghosh, B., and Konar, R., (2012) Textural developments in chromite deforming under eclogite-facies conditions from the Neoarchaean Sittampundi anorthosite complex, southern India. Geological Journal, 47, 253-262.

Ghosh, B., Ray, J., and Morishita, T., (2014) Grain-scale plastic deformation of chromite from podiform chromitite of the Naga–Manipur ophiolite belt, India.: Implication to mantle dynamics. Ore Geology Reviews, 56, 199–208.

Gottstein, G., and Shvindlerman, L.S. (2010) Grain Boundary Migration in Metals: Thermodynamics, Kinetics, Applications, 2nd ed., CRC Press, Boca Raton, FL.

Halfpenny, A., Prior, D.J., and Wheeler, J., (2006) Analysis of dynamic recrystallization and nucleation in a quartzite mylonite. Tectonophysics, 427, 3-14.

Halfpenny, A., Prior, D.J., and Wheeler, J., (2012) Electron backscatter diffraction analysis to determine the mechanisms that operated during dynamic recrystallisation of quartz-rich rocks. Journal of Structural Geology, 36, 2-15.

Hay, R.S., and Evans, B., (1987) Chemically induced grain boundary migration in calcite: temperature dependence, phenomenology, and possible applications to geologic systems. Contributions to Mineralogy and Petrology, 97, 127-141.

Hirth, G., and Kohlstedt, D.L., (1995) Experimental constraints on the dynamics of the partially molten upper mantle: Deformation in the diffusion creep regime. Journal of Geophysical Research, 100(B2), 1981–2001.

Hirth, G., and Tullis, J., (1992) Dislocation creep regimes in quartz aggregates. Journal of Structural Geology, 14, 145-159.

Humphreys, F.J., and Hatherly, M., (1995) Recrystallization and related annealing phenomena. Oxford, Pergamon.

Kang, S.J.L., (2005). Sintering: densification, grain growth, and microstructure. Elsevier, Butterworth-Heinemann.

Kirby, S.H., and Kronenberg, A.K., (1984) Diffusion induced grain boundary motion (DIGM) and diffusion induced recrystallization (DIR): applications to the rheology of rocks. Eos, Transactions American Geophysical Union, 65, 1098.

Meissner, B., Deters, P., Srikantappa, C., and Köhler, H., (2002) Geochronological evolution of the Moyar, Bhavani and Palghat shear zones of southern India: implications for East Gondwana correlations. Precambrian Research, 114, 149–175.

Naidu, P.R.J., (1963) A layered complex in Sittampundi, Madras state, India. Mineralogical Society of America Special Paper 1, 116–123.

Omori, T., Kusama, T., Kawata, S., Ohnuma, I., Sutou, Y., Araki, Y., Ishida, K., and Kainuma, R., (2013) Abnormal Grain Growth Induced by Cyclic Heat Treatment. Science, 341, 1500-1502.

Ozawa, K., (1985) Olivine-spinel geospeedometry: Analysis of diffusion-controlled Mg-Fe^{2+} exchange. Geochimica et Cosmochimica Acta, 48, 2597-2611.

Ozawa, K., (1989) Stress-induced Al–Cr zoning of spinel in deformed peridotites. Nature, 338, 141– 144.

Passchier, C.W., and Trouw, R.A.J., (2005) Microtectonics, 2nd edn. Springer, Berlin.

Piazolo, S., Bestmann, M., Prior, D.J., and Spiers, C.J., (2006) Temperature dependent grain boundary migration in deformed-then-annealed material: Observations from experimentally deformed synthetic rocksalt. Tectonophysics, 427, 55-71.

Piazolo, S., Prior, D.J., and Holness, M.D., (2005) The use of combined Cathodoluminescence and EBSD analysis: A case study investigating grain boundary migration mechanisms in quartz. Journal of Microscopy, 217, 152-161.

Prior, D.J., Wheeler, J., Brenker, F.E., Harte, B., and Matthews, M., (2000) Crystal plasticity of natural garnet: New microstructural evidence. Geology, 28, 1003-1006.

Poirier, J-P., (1985) Creep of Crystals. Cambridge University Press, Cambridge.

Ramadurai, S., Sankaran, M., Selvan, T.A., and Windley, B.F., (1975) The stratigraphy and structure of the Sittampundi complex, Tamil Nadu. Journal of the Geological Society of India, 16, 409–414.

Sajeev, K., Windley, B.F., Connolly, J.A.D., and Kon, Y., (2009) Retrogressed eclogite (20 kbar, 1020°C) from the Neoproterozoic Palghat–Cauvery suture zone, southern India. Precambrian Research, 171, 23–36.

Sammis, C.G., (1989) Stress-induced segregation. Nature, 338, 114-115.

Santosh, M., and Kusky, T., (2010) Origin of paired high pressure–ultrahigh temperature orogens: a ridge subduction and slab window model. Terra Nova, 22, 35-42.

Santosh, M., Maruyama, S., and Sato, K., (2009) Anatomy of a Cambrian suture in Gondwana: Pacific-type orogeny in southern India? Gondwana Research, 16, 321-341.

Santosh, M., and Sajeev, K., (2006) Anticlockwise evolution of ultrahigh-temperature granulites within continental collision zone in southern India. Lithos, 92, 447-464.

Satsukawa, T., Piazolo, S., González-Jiménez, J.M., Colás, V., Griffin, W.L., O'Reilly, S.Y., Gervilla, F., Fanlo, I., and Kerestedjian, T N., (2015a) Fluid-present deformation aids chemical modification of chromite: Insights from chromites from Golyamo Kamenyane, SE Bulgaria. Lithos, 228, 78-89.

Satsukawa T., Griffin, W.L., Piazolo, S. and O'Reilly, S.Y., (2015b) Messengers from the deep:Fossil wadsleyite-chromite microstructures from the Mantle Transition Zone. Scientific Reports, 5, doi:10.1038/srep16484.

Smit, M.A., Scherer, E.E., John, T., and Janssen, A., (2011) Creep of garnet in eclogite: Mechanisms and implications. Earth and Planetary Science Letters, 311, 411-419.

Stöckhert, B., and Duyster, J., (1999) Discontinuous grain growth in recrystallised vein quartz-implications for grain boundary structure, grain boundary mobility, crystallographic preferred orientation, and stress history. Journal of Structural Geology, 21, 1477-1490.

Storey, C.D., and Prior, D.J., (2005) Plastic deformation and recrystallization of garnet: a mechanism to facilitate diffusion creep. Journal of Petrology, 46, 2593-2613.

Stunitz, H., (1998) Syndeformational recrystallization – dynamic or compositionally induced? Contributions to Mineralogy and Petrology, 131, 219-236.

Subramaniam, A.P., (1956) Mineralogy and petrology of the Sittampundi complex, Salem district, Madras State, India. Bulletin Geological Society of America, 67, 317–390.

Suita, M.T., and Streider, A.J., (1996) Cr-spinels from Brazilian mafic-ultramafic complexes: metamorphic modifications. International Geology Review, 38, 245–267.

Toriumi, M., and Karato, S., (1985) Preferred orientation development of dynamically recrystallized olivine during high temperature creep. Journal of Geology, 93, 407-417.

Tullis, J., and Yund, R.A., (1985) Dynamic recrystallization of feldspar: a mechanism for ductile shear zone formation. Geology, 13, 238-241.

Urai, J.L., (1983) Water assisted dynamic recrystallization and weakening in polycrystalline bischofite. Tectonophysics, 96, 125-157.

Urai, J.L., Means, W.D., and Lister, G.S., (1986) Dynamic recrystallization of minerals, in, Hobbs, B.E., and Heard, H.C., eds., Mineral and rock deformation: laboratory studies. American Geophysical Union Monograph, 36, 161-199.

Vukmanovic, Z., Barnes, S.J., Reddy S.M., Godel, B., and Fiorentini, M.L., (2013) Morphology and microstructure of chromite crystals in chromitites from the Merensky Reef (Bushveld Complex, South Africa). Contributions to Mineralogy and Petrology, 165, 1031-1050.

Wang, Z., and Ji, S., (2000) Diffusion creep of fine-grained garnetite: implications for the flow strength of subducting slabs. Geophysical Research Letters, 27, 2333-2336.

White, S.H., (1975) Tectonic deformation and recrystallization of oligoclase. Contributions to Mineralogy and Petrology, 50, 287-304.

Wood, B.J., and Virgo, D., (1989) Upper mantle oxidation state: ferric iron contents of lherzolite spinels by ^{57}Fe Mossbauer spectroscopy and resultant oxygen fugacities. Geochimica et Cosmochimica Acta, 53, 1277-1291.

Yund, R.A., and Tullis, J., (1991) Compositional changes of minerals associated with dynamic recrystallization. Contributions to Mineralogy and Petrology, 108, 346-355.

Figure Captions

FIGURE 1. (A) The generalized geological map of Sittampundi Layered Complex (modified from Subramaniam, 1956) showing disposition of various lithomembers. The inset map (after Santosh and Sajeev, 2006) shows tectonic framework of southern India. PCSZ: Palghat–Cauvery Suture Zone; CSZ: Chennamalai Shear Zone; ACSZ: Achankovil Shear Zone. (B) The exposures of the chromite seams in the field at three different locations (marked by different symbols in A) used in this study. Sample location KPT5, BL-SII and CPT6 occur stratigraphically in upper, middle and lower horizons, respectively.

FIGURE 2. A schematic representation of the sample processing and geometry for the EBSD analysis. (A) The foliation plane was set to A1-A2 plane and cut perpendicular to the A1 axis for observation on A2-A3 plane. (B) The sample (shaded area in A) then prepared for the EBSD analysis and placed in the SEM chamber for data collection keeping A1 axis projected towards the phosphor screen.

FIGURE 3. EBSD analysis for sample KPT5. Dark grey tones in these maps represent non-indexed areas dominated by amphibole. (A)-(C) Image quality (IQ), inverse pole figure (IPF), projected along the z direction, and kernel average misorientation (KAM) maps, respectively showing concentration of the deformation at the parent grain boundary. B and C also mark the subgrain, intermediate grain and recrystallized grain boundaries following the definition provided in the text. (D) The texture-component map considering orientations ranging within 30° from the orientation of the parent grain measured at the center. The orientations within 30° are coloured proving that the origin of the subgrains are from the parent grains. (E) Misorientation profiles showing the gradual change of misorientations relative to the first point (considering 0°

misorientation) of the profile. The misorientation values are added to the first point with the direction of transect. Individual profiles are highlighted by different color with reference to the profile lines shown by arrowheads in (A).

FIGURE 4. EBSD analysis for sample KPT5. The description of individual figures and illustrations (A-E) are similar to those given in Figure 3.

FIGURE 5. EBSD analysis for sample BL-SII. The description of individual figures and illustrations (A-E) are similar to those given in Figure 3. Note the development of new recrystallized (neighbor-daughter) grains along the boundaries of the parent grains. The KAM map (C) shows the new grains are strain free and form 120° triple junctions. Their internal misorientation angle is less than 1° (E, inset). In (D), five parent grains are indemnified (marked with 1-5) in the texture-component maps; coded with similar color effect (rainbow) performed in separate steps.

FIGURE 6. EBSD analysis for sample BL-SII. The description of individual figures and illustrations (A-E) are similar to those given in Figure 3. The growth initiation of strain-free grains at the edge of the parent grains are marked by white arrowheads. The misorientation angles also increased and the boundaries are marked by sharp jumps (E).

FIGURE 7. EBSD analysis for sample CPT6. The description of individual figures and illustrations (A-D and F) are similar to those given in Figure 3. The white arrowheads in B point to the new strain free "abnormal grain growths". In D, two such crystals are marked with plane trace overlay showing the orientation of the crystal for {111} planes.

FIGURE 8. EBSD analysis for sample CPT6. The description of individual figures and illustrations (A-C) are similar to those given in Figure 3. The abnormal grain growth and intense deformation in the parent grain is prominent. The transects show a general trend of increasing misorientation angles from the core to edge of the parent grain (D), however, sharp jump of misorientation is common. Unlike the other abnormal grain growths, shown in Figure 7, one grain in this section shows week deformation by showing the development of feeble sub-grain boundary (highlighted by dashed line in A and pointed by white arrowhead). This is further confirmed by the transect misorientation data shown in (E) and (F).

FIGURE 9. The high contrast BSE image (sample location CPT6) at the top represents overall compositional heterogeneity in terms of tonal difference. The boundaries of the recrystallized, strain-free new grains are shown by yellow dashed lines. Note, the Cr# value is less in the new grains compared to the parent grain. The four plates at the bottom show compositional maps (X-ray) of the same sample. Note, the distribution of Cr and Al has a variation across the region, while Mg and Fe does not show any spatial change.

FIGURE 10. A schematic illustrations showing chemical diffusion at very high-angle grain boundary of one faceted new grain. This grain grows at the expense of subgrains by outward migration of its high-angle grain boundaries. At the left illustration, I, II, III, IV are representing parent-grain, subgrain, neighbor-daughter and abnormal grain growths, respectively. At the left, HAGB and LAGB are indicating high-angle and low-angle grain boundaries, respectively.

This is a preprint, the final version is subject to change, of the American Mineralogist (MSA)
Cite as Authors (Year) Title. American Mineralogist, in press.
(DOI will not work until issue is live.) DOI: http://dx.doi.org/10.2138/am-2017-5709

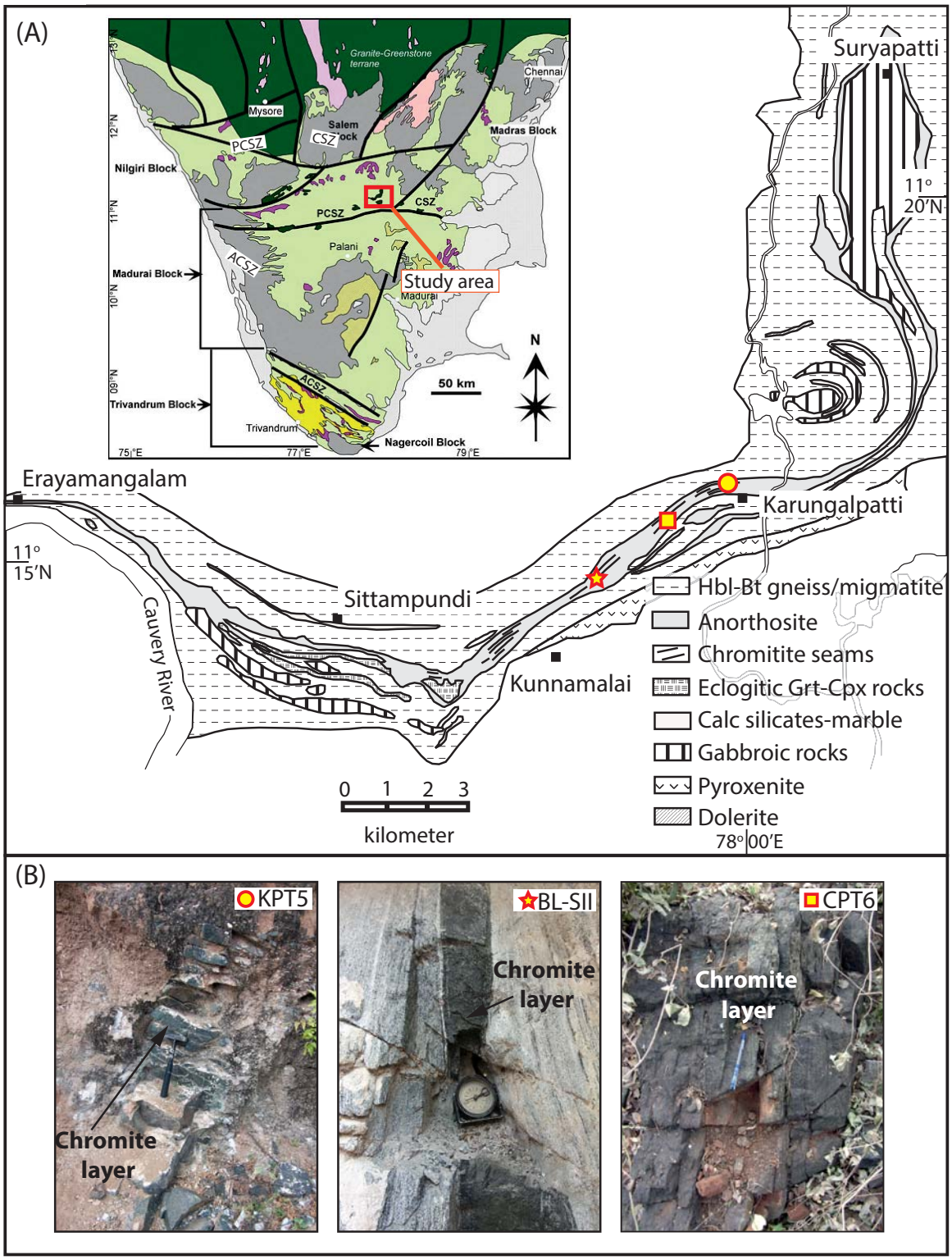

Figure 1

This is a preprint, the final version is subject to change, of the American Mineralogist (MSA)
Cite as Authors (Year) Title. American Mineralogist, in press.
(DOI will not work until issue is live.) DOI: http://dx.doi.org/10.2138/am-2017-5709

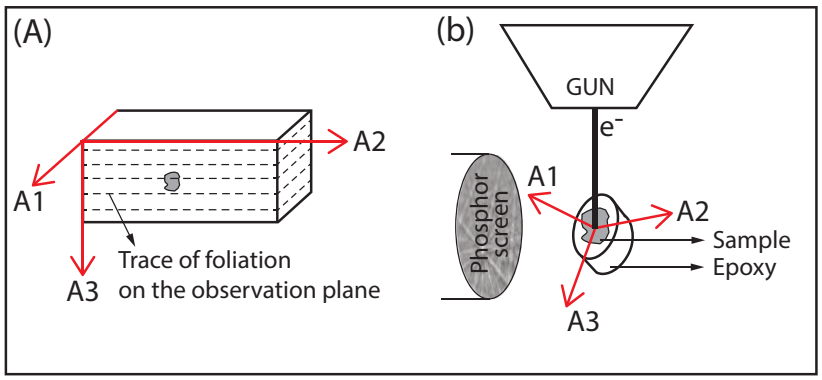

Figure 2

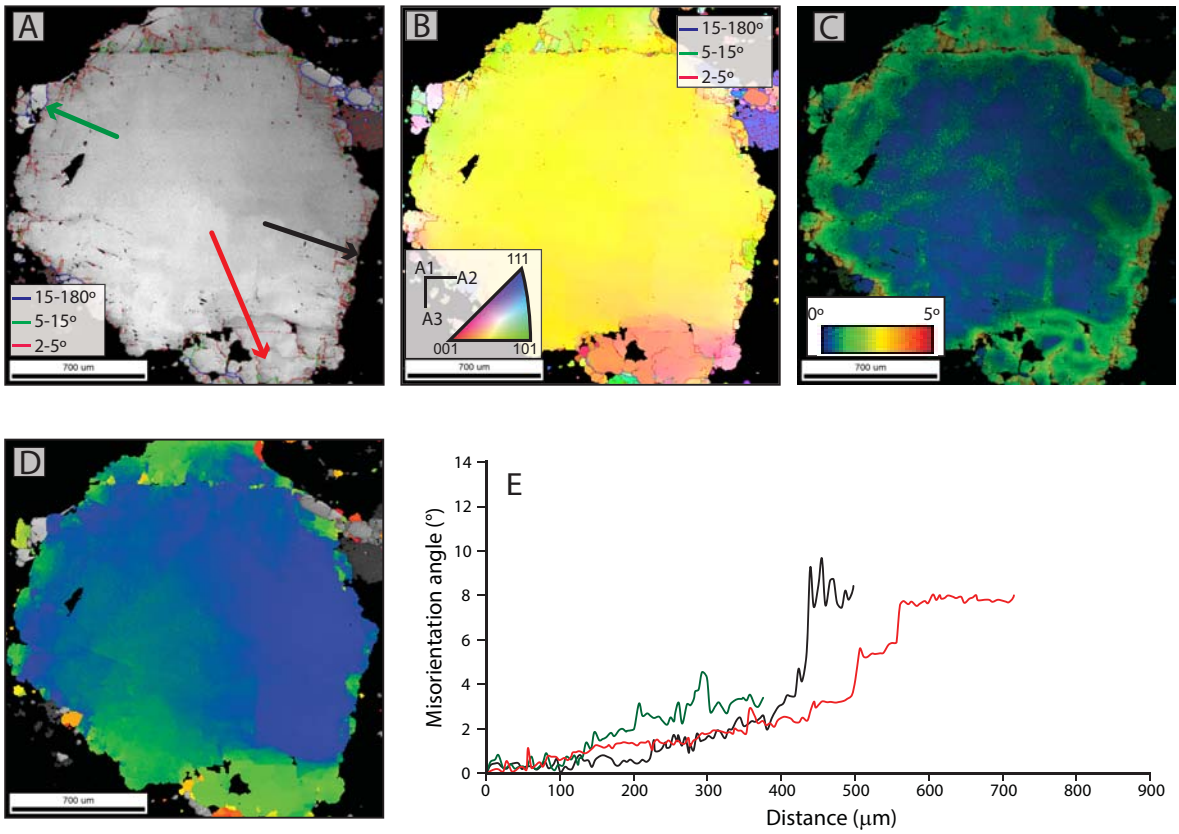

Figure 3

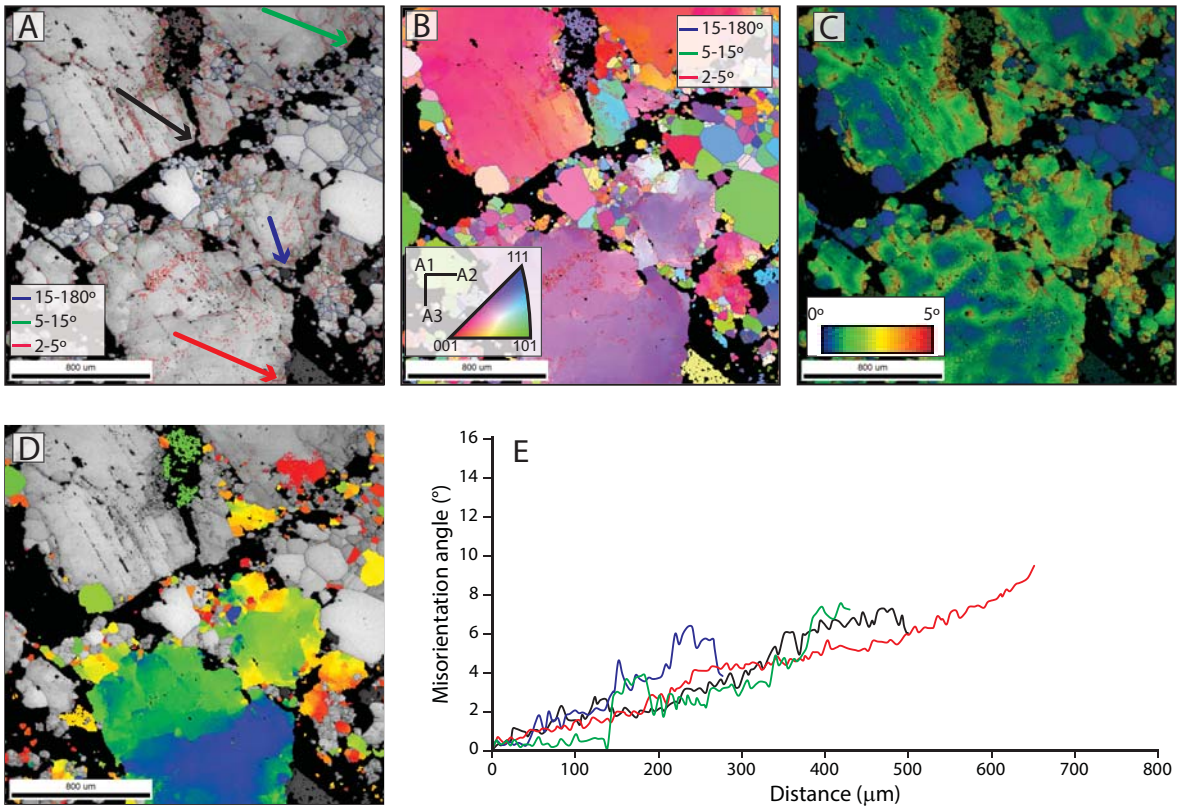

Figure 4

This is a preprint, the final version is subject to change, of the American Mineralogist (MSA)
Cite as Authors (Year) Title. American Mineralogist, in press.
(DOI will not work until issue is live.) DOI: http://dx.doi.org/10.2138/am-2017-5709

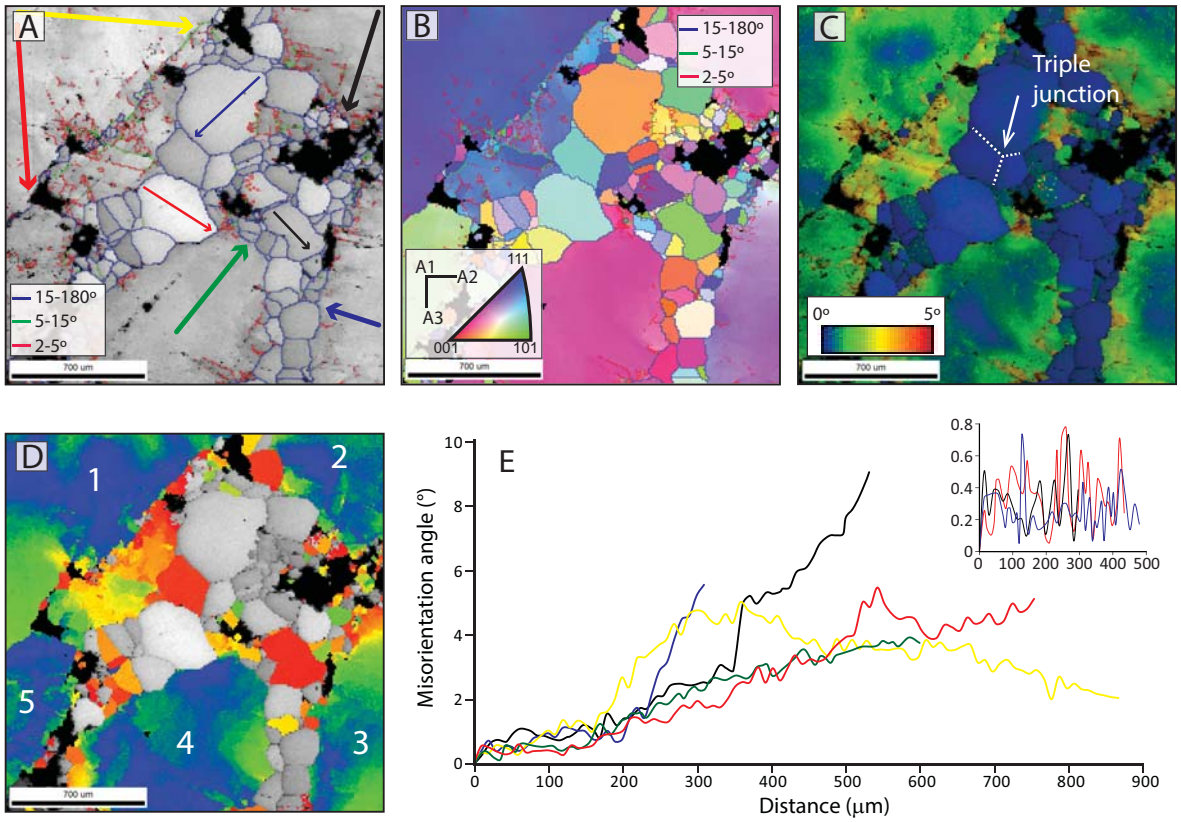

Figure 5

This is a preprint, the final version is subject to change, of the American Mineralogist (MSA)
Cite as Authors (Year) Title. American Mineralogist, in press.
(DOI will not work until issue is live.) DOI: http://dx.doi.org/10.2138/am-2017-5709

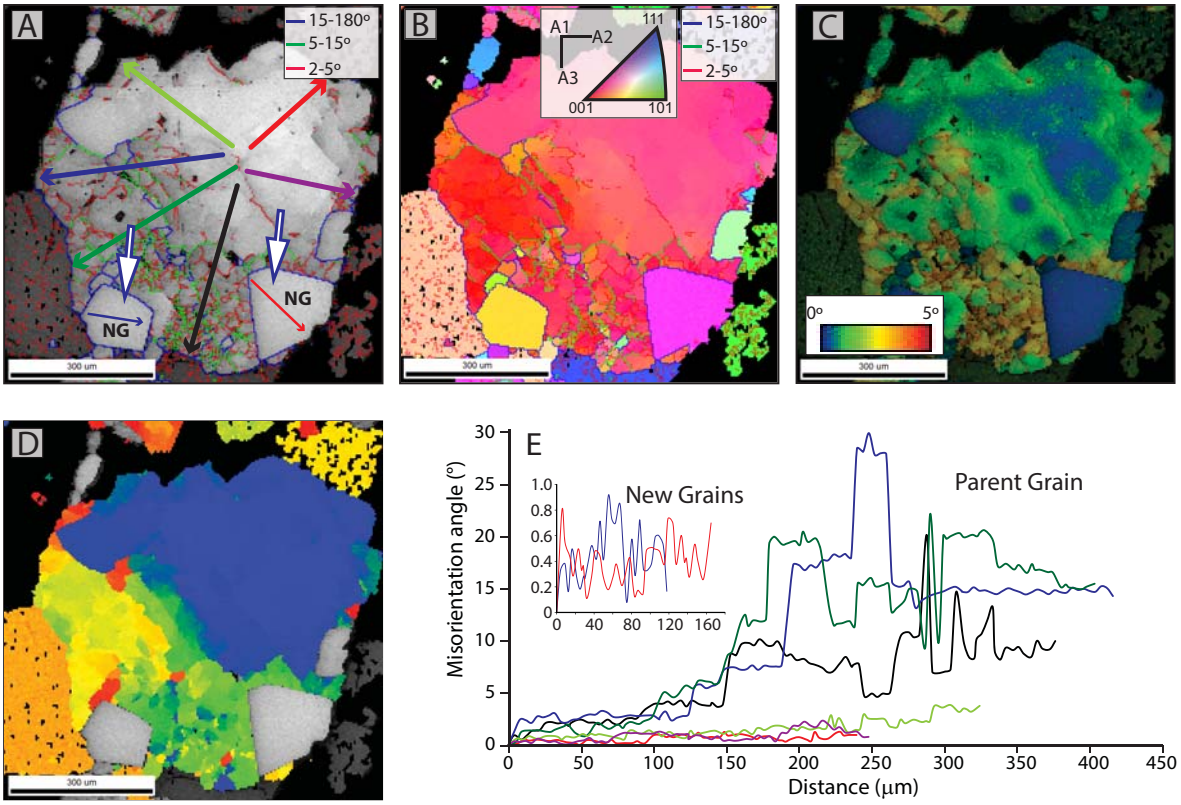

Figure 6

This is a preprint, the final version is subject to change, of the American Mineralogist (MSA)
Cite as Authors (Year) Title. American Mineralogist, in press.
(DOI will not work until issue is live.) DOI: http://dx.doi.org/10.2138/am-2017-5709

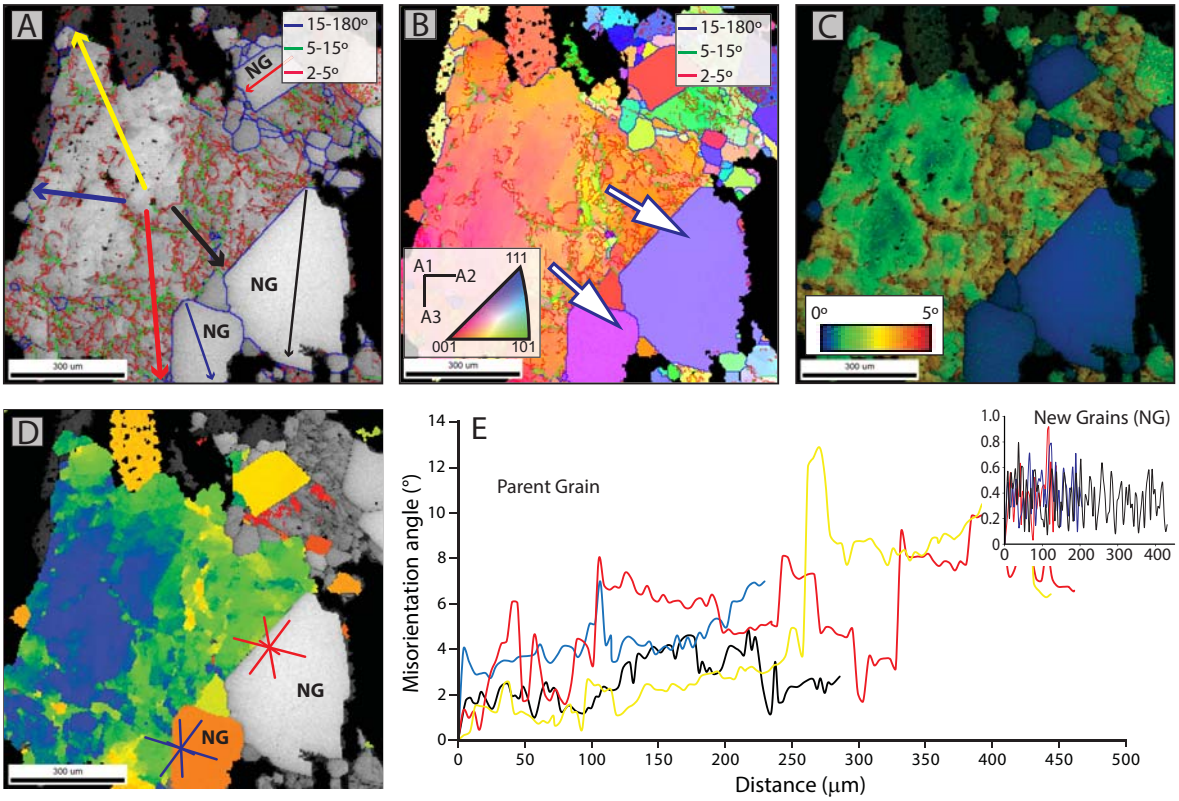

Figure 7

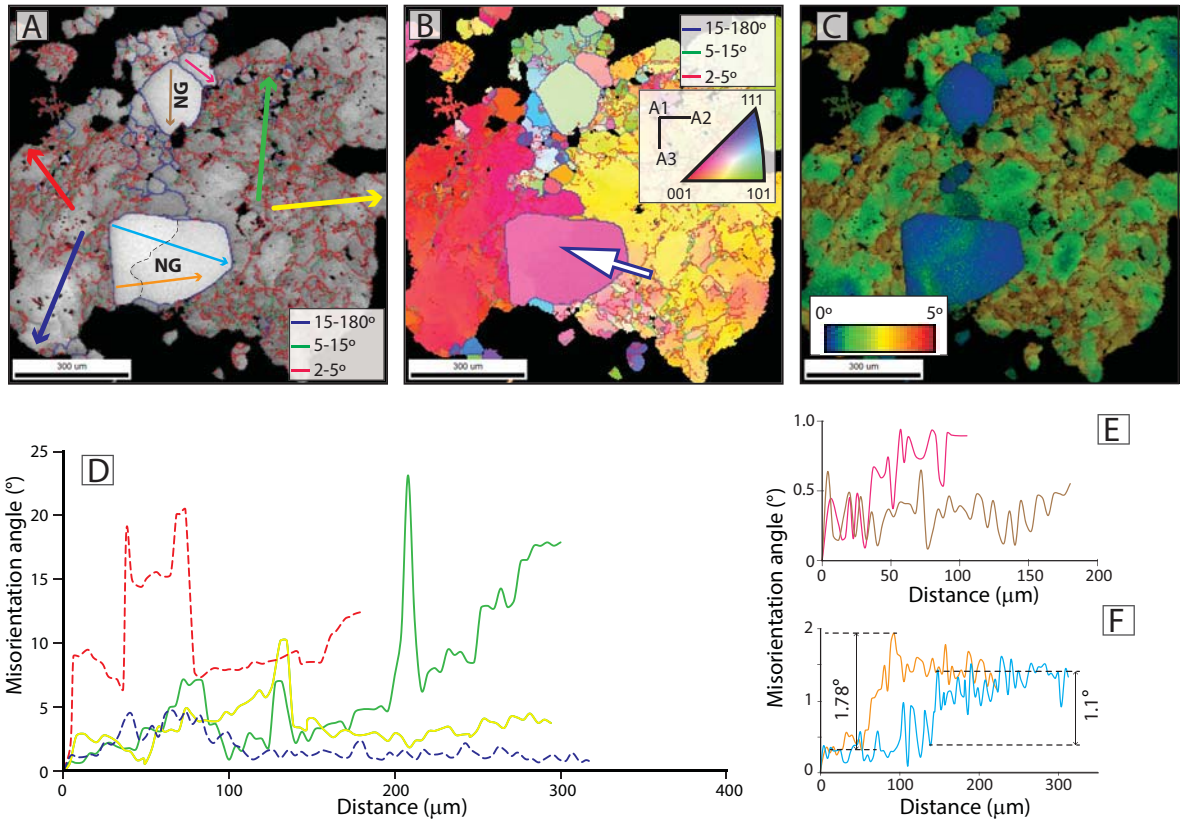

Figure 8

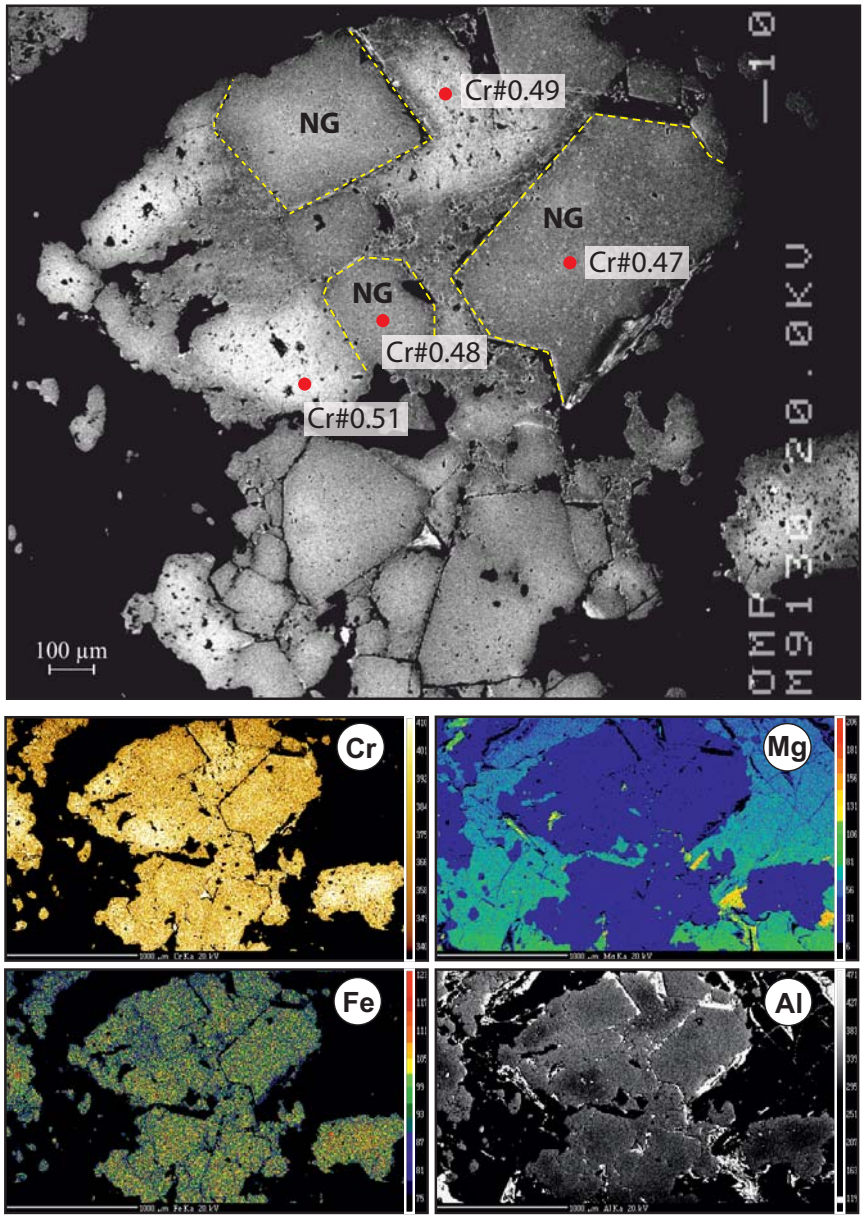

Figure 9

This is a preprint, the final version is subject to change, of the American Mineralogist (MSA)
Cite as Authors (Year) Title. American Mineralogist, in press.
(DOI will not work until issue is live.) DOI: http://dx.doi.org/10.2138/am-2017-5709

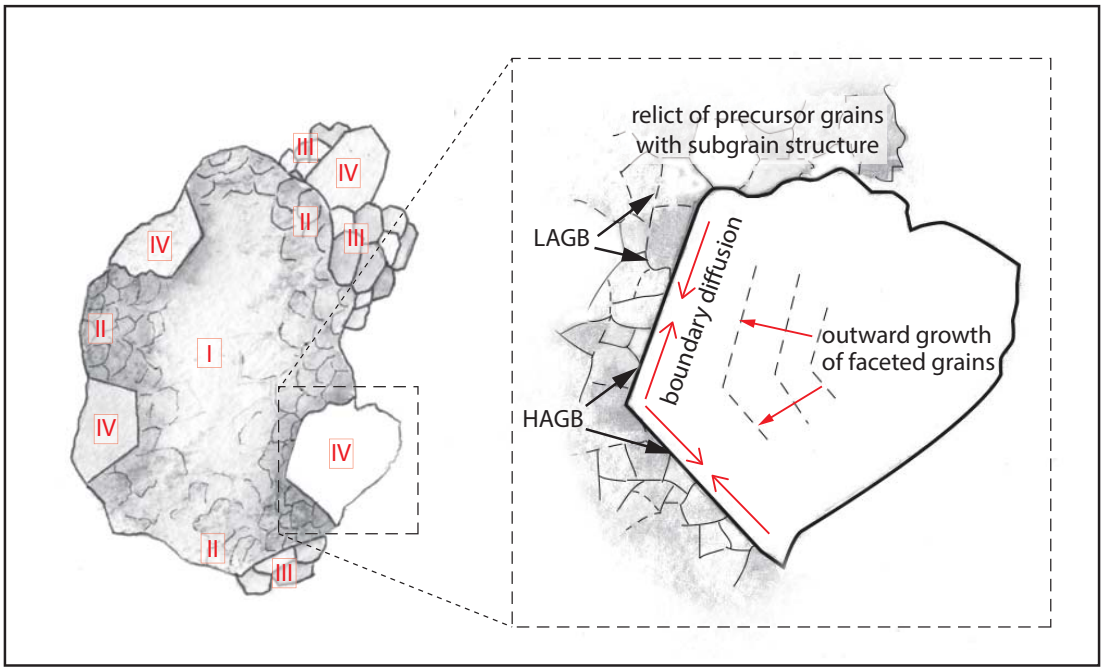

Figure 10